Nano Materials Science 3 (2021) 68–74

Contents lists available at ScienceDirect

Nano Materials Science

journal homepage: www.keaipublishing.com/cn/journals/nano-materials-science/

Free-standing flexible graphene-based aerogel film with high energy density as an electrode for supercapacitors

Shijia Yuan [a], Wei Fan [a,*], Yanan Jin [c], Dong Wang [a], Tianxi Liu [a,b,**]

[a] State Key Laboratory for Modification of Chemical Fibers and Polymer Materials, College of Materials Science and Engineering, Innovation Center for Textile Science and Technology, Donghua University, 2999 North Renmin Road, Shanghai, 201620, PR China
[b] Key Laboratory of Synthetic and Biological Colloids, Ministry of Education, School of Chemical and Material Engineering, Jiangnan University, Wuxi, 214122, PR China
[c] Key Laboratory for Special Functional Materials of Ministry of Education, National & Local Joint Engineering Research Centre for High-efficiency Display and Lighting Technology, School of Materials and Engineering, Collaborative Innovation Centre of Nano Functional Materials and Applications, Henan University, Kaifeng, 475004, PR China

ARTICLE INFO

Keywords:
Graphene
Aerogel film
Polypyrrole
N-doping
Supercapacitor

ABSTRACT

Two-dimensional graphene film exhibits sluggish ion diffusivity while three-dimensional (3D) graphene aerogel has low packing density and poor mechanical flexibility. Consequently, there is an urgent need for graphene-based film with both mechanical robustness and high specific capacitance. Here, we present an easy and scalable strategy for fabricating a free-standing flexible graphene-based aerogel film electrode with a two-layered structure, in which the top layer is an interconnected macroporous reduced graphene oxide/carbon nanotube (RGO/CNT) aerogel, and the bottom layer is a flexible electrospun polyacrylonitrile (PAN) nanofiber membrane. The porous 3D structure of the aerogel provides fast transport of electrolyte ions and electrons, while the nanofiber membrane provides both strong support for the aerogel and mechanical flexibility. Polypyrrole (PPy) can be uniformly loaded on RGO/CNT/PAN (RCP) composite aerogel film to provide pseudocapacitance, and nitrogen-doped RGO/CNT/carbon nanofiber (NRCC) aerogel film can be obtained by further pyrolysis. The resultant RCP@PPy-0.05//NRCC based asymmetric supercapacitor can have a maximum voltage of 1.7 V and a maximum energy density of 60.6 W h kg^{-1} at 850.2 W kg^{-1}. This indicates that free-standing graphene-based aerogel film can be used in flexible supercapacitors.

1. Introduction

With the increasing popularity of wearable electronic devices, flexible and lightweight supercapacitors have become hot research topics as flexible electrodes with high capacitance are crucial for wearable and flexible supercapacitors with high energy density. Free-standing graphene film is considered an ideal electrode for flexible supercapacitors because of its large surface area, excellent electrical conductivity, and good mechanical properties [1–4]. In addition, it remains stable without additional binders, which enables further improvement in the overall electrochemical performance of the electrode [5–8]. Presently, there are three main methods for preparing free-standing graphene film: chemical vapor deposition (CVD) [9–12], template-assisted preparation [13–15] and vacuum-assisted self-assembly of graphene oxide (GO) [16]. However, the graphene film produced by these methods usually forms a dense two-dimensional (2D) layered structure due to the restacking of the graphene sheets via van der Waals attractions and π-π stacking [7,17,18]. Due to the decreased surface area and long mass transport length, this compact stacked graphene electrode exhibits greatly limited cross-plane ion diffusivity and a sluggish kinetic response, resulting in poor capacitive behavior, especially at high charging rates.

Studies have shown that graphene, such as the graphene aerogel, can give full play to its excellent properties in the three-dimensional (3D) porous structure by combining the structural characteristic of the aerogel and the physicochemical properties of the graphene [19–21]. Currently, the self-assembly method of GO is the most common strategy for fabricating 3D graphene aerogel, with the gelation of GO followed by reduction being the most effective and simplest method. Bai et al. reported a study on GO gelation [11,22]. The GO dispersion turns into a gel state when the balance between the van der Waals force and the

* Corresponding author.
** Corresponding author. State Key Laboratory for Modification of Chemical Fibers and Polymer Materials, College of Materials Science and Engineering, Innovation Center for Textile Science and Technology, Donghua University, 2999 North Renmin Road, Shanghai, 201620, PR China.
E-mail addresses: weifan@dhu.edu.cn (W. Fan), txliu@dhu.edu.cn, txliu@fudan.edu.cn (T. Liu).

https://doi.org/10.1016/j.nanoms.2020.03.003
Received 4 January 2020; Accepted 25 February 2020
Available online 26 March 2020
2589-9651/© 2020 Chongqing University. Production and hosting by Elsevier B.V. on behalf of KeAi. This is an open access article under the CC BY-NC-ND license (http://creativecommons.org/licenses/by-nc-nd/4.0/).

electrostatic repulsion is broken. During the gelation process, a portion of the GO sheets tends to overlap to form GO hydrogel with a 3D structure, and the GO hydrogel is further reduced to obtain a 3D reduced graphene oxide (RGO) network. Adding spacers between the graphene sheets can prevent the GO sheets from restacking and promote the construction of a 3D graphene network structure, including carbon nanotubes (CNTs) [23–26], nanoparticles [27,28] and polymers [29–31]. For example, Wu et al. produced chemically converted graphene and polyaniline nanofiber composite film, in which polyaniline nanofibers were uniformly sandwiched between graphene layers [29]. Huang et al. synthesized a porous graphene aerogel using silica spheres and GO as raw materials [28]. Sun et al. used a mixed solution of CNTs and GO sheets as precursors to fabricate ultra-flyweight aerogel through freeze-drying and carbonization [26]. Even though the graphene-based aerogel prepared at present has good electrochemical performance in the presence of spacers, it still shows low packing density leading to poor energy density, as well as poor flexibility that cannot be directly fabricated into flexible electrodes. Hence, engineering a desirable graphene film with both mechanical flexibility and high specific capacitance remains a challenge. Thus, it is necessary to design graphene electrode materials with the properties needed to meet this challenge, including high packing density, good flexibility, fast ion diffusion and small internal resistance.

Here, we demonstrate a scalable and cost-effective strategy to prepare 3D graphene aerogel film. Electrospun polyacrylonitrile (PAN) nanofiber membrane was used as a flexible substrate, on which GO/CNT gel was coated to construct a 3D porous structure. Free-standing GO/CNT/PAN (GCP) aerogel film consisting of a bottom PAN nanofiber membrane providing flexibility and strong support for the upper aerogel, and an upper GO/CNT aerogel that displays an interconnected macroporous structure facilitating rapid transport of electrolyte ions and electrons was obtained by freeze-drying. Polypyrrole (PPy) was uniformly loaded on the GCP aerogel film to introduce pseudocapacitance, and free-standing RGO/CNT/PAN@PPy (RCP@PPy) composite aerogel film was produced after reduction. Nitrogen-doped RGO/CNT/carbon nanofiber (NRCC) composite aerogel film was obtained after further pyrolysis at high temperature. The free-standing RCP@PPy composite aerogel film was assembled into symmetric supercapacitors with a maximum specific capacity of 716 F g^{-1}, which were assembled with RCP@PPy as the positive electrode and NRCC as the negative electrode, achieving a maximum energy density of 60.6 W h kg^{-1} at 850.2 W kg^{-1}. The free-standing flexible graphene-based aerogel film electrode exhibits excellent electrochemical performance, and can potentially be applied in wearable supercapacitors.

2. Experiment

2.1. Preparation of free-standing GO/CNT/PAN (GCP) composite aerogel film

2 g of PAN powder was dissolved in 10 g of N,N-dimethylformamide (DMF) and stirred for several hours until the PAN was fully dissolved to obtain a PAN spinning solution. The electrospinning was performed with a voltage of 20 kV and a feeding rate of 0.25 mm min^{-1}. Then the electrospun PAN nanofiber membrane was placed in an oven raised to 250 °C with a heating rate of 1 °C min^{-1}, and kept at 250 °C for 1 h to obtain the pre-oxidized PAN membrane.

Stable GO/CNT hybrid hydrogel was prepared as follows. GO was prepared by a modified Hummers' method [32] and configured into a suspension (6 mg mL^{-1}). Then 3 mg mL^{-1} CNT suspension was mixed with GO suspension (volume ratio of 1:1) and ultrasonicated for 3 h to obtain a GO/CNT hybrid hydrogel. Afterwards, the GO/CNT hydrogel was dripped onto the pre-oxidized PAN nanofiber membrane and the gel was evenly coated on the membrane using a coating machine. The thickness of the aerogel layer was controlled by adjusting the amount of gel. After keeping still for 1 h and freeze-drying for 12 h, a free-standing GO/CNT/PAN (GCP) composite aerogel film was obtained. After reducing the GCP composite aerogel film through a mixed solution of HI and HAc (volume ratio 1:2), the obtained composite aerogel film was named RGO/CNT/PAN (abbreviated as RCP).

2.2. Synthesis of free-standing RGO/CNT/PAN@PPy (RCP@PPy) and N-doped RGO/CNT/CNF (NRCC) composite aerogel film

The pyrrole monomer was dispersed in 1 M HCl solution and cooled in an ice water bath. The previously prepared GCP composite aerogel film was fully immersed in the solution. Ammonium persulfate (APS) (APS with a mass ratio of 1:1 to pyrrolesolution) was slowly dripped into the above dispersion to initiate the polymerization of the pyrrole. After the polymerization was completed, the composite film was washed repeatedly with DI water and ethanol. Next, the GO/CNT/PAN@PPy composite film was reduced with a mixed solution of HI and HAc. Finally, free-standing RGO/CNT/PAN@PPy composite aerogel film was produced after washing and drying under vacuum. The loading amount of polypyrrole was adjusted by varying the concentration of pyrrole (0.01, 0.05, and 0.1 mol L^{-1}), and the corresponding composite films were named RGO/CNT/PAN@PPy-x (abbreviated as RCP@PPy-x, x = 0.01, 0.05, 0.1). Among them, RCP@PPy-0.05 was selected as the precursor film and was then carbonized in N_2 atmosphere at 600 °C for 2 h. The carbonized aerogel film was named N-doped RGO/CNT/CNF (abbreviated as NRCC).

2.3. Electrochemical measurements

Electrochemical testing was done on the CHI 660D electrochemical workstation. In the two-electrode testing system, a sample was uniformly cut into 10 × 10 mm^2 squares to prepare an electrode. Using filter paper as the separator and carbon paper (0.2 mm thick) as the current collector, the test was completed in a 0.5 M H_2SO_4 electrolyte. RCP, RCP@PPy-x and NRCC samples were assembled into symmetric super-capacitors. The test voltage range of the constant current charge and discharge curve (GCD) at different current densities was consistent with the cyclic voltammetry (CV) curve (0–1 V, -1-0 V). Electrochemical impedance spectroscopy (EIS) was measured at an amplitude of 5 mV and a frequency of 0.01–10 kHz. The specific capacitance of a single electrode was calculated using the following equation:

$$C = \frac{2It}{mV} \tag{1}$$

where I represents the discharge current (A), t represents the discharge time (s), m represents the total mass (g) of the electrode, and V represents the voltage window.

RCP@PPy-0.05//NRCC asymmetric supercapacitor performance test: An RCP@PPy-0.05 sample was used as the positive electrode and an NRCC sample was used as the negative electrode. The test voltage range: 0–1.7 V. The mass ratio of the RCP@PPy-0.05 sample to the NRCC sample was 0.49 calculated by the following equation:

$$\frac{m_+}{m_-} = \frac{C_- \times V_-}{C_+ \times V_+} \tag{2}$$

where C represents the specific capacitance (F g^{-1}), V represents the operating voltage (V), and m represents the mass (g) of the electrode.

The energy density (E, Wh Kg^{-1}) and power density (P, W Kg^{-1}) can be calculated from the following equations:

$$E = \frac{\frac{1}{2}CV^2}{3.6} \tag{3}$$

$$P = \frac{3600E}{t} \tag{4}$$

where C represents the specific capacitance (F g^{-1}) of the asymmetric supercapacitor, V represents the operating voltage (V), and t represents the discharge time (s).

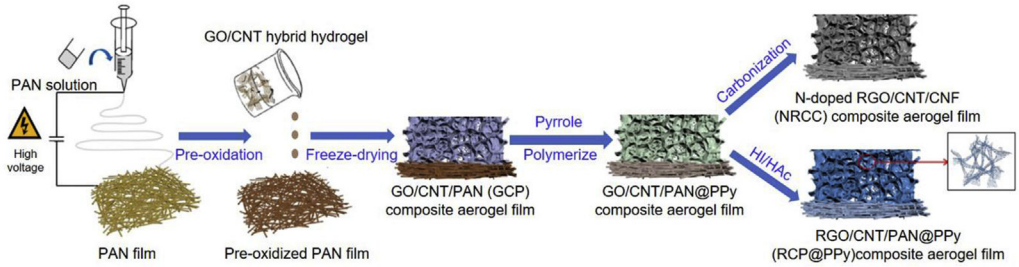

Fig. 1. Schematic illustration of the fabrication of RCP@PPy-x and NRCC.

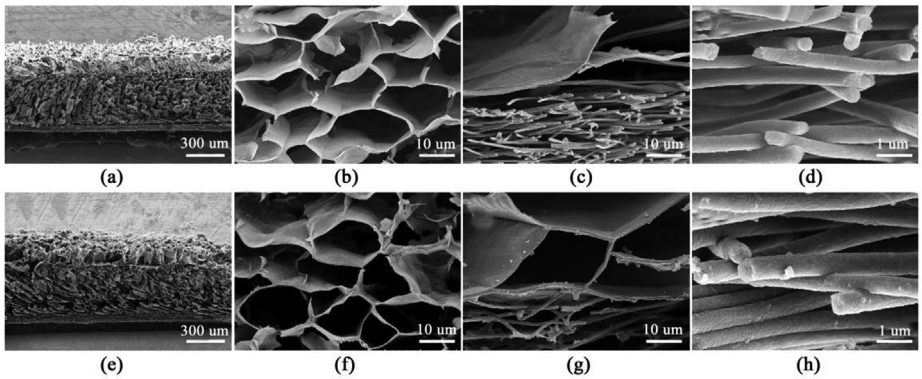

Fig. 2. SEM images of RCP (a–d), RCP@PPy-0.05 (e–f). (a, e) Cross-section of the film; (b, f) Upper-section of the composite aerogel; (c, g) Middle-section and (d, h) Bottom-section of the PAN nanofiber.

3. Results and discussion

3.1. Morphology and chemical characterization of RCP@PPy-x and NRCC aerogel film

Here, we used a flexible PAN nanofiber membrane as the substrate on which to construct a GO/CNT gel network. A free-standing composite aerogel film was obtained after freeze-drying. The schematic illustration is presented in Fig. 1. The PAN nanofiber membrane was obtained by electrospinning and was pre-oxidized to enhance its hydrophilicity. It can be seen that the PAN membrane can be curled and used as a flexible substrate (Fig. S1a). GO/CNT hybrid gel was coated on the PAN nanofiber membrane to construct a 3D porous structure, resulting in a free-standing GO/CNT/PAN (GCP) composite aerogel film. The GCP composite aerogel film is flexible and bendable, and the area and shape can vary with the size and shape of the flexible PAN substrate (Fig. S1b).

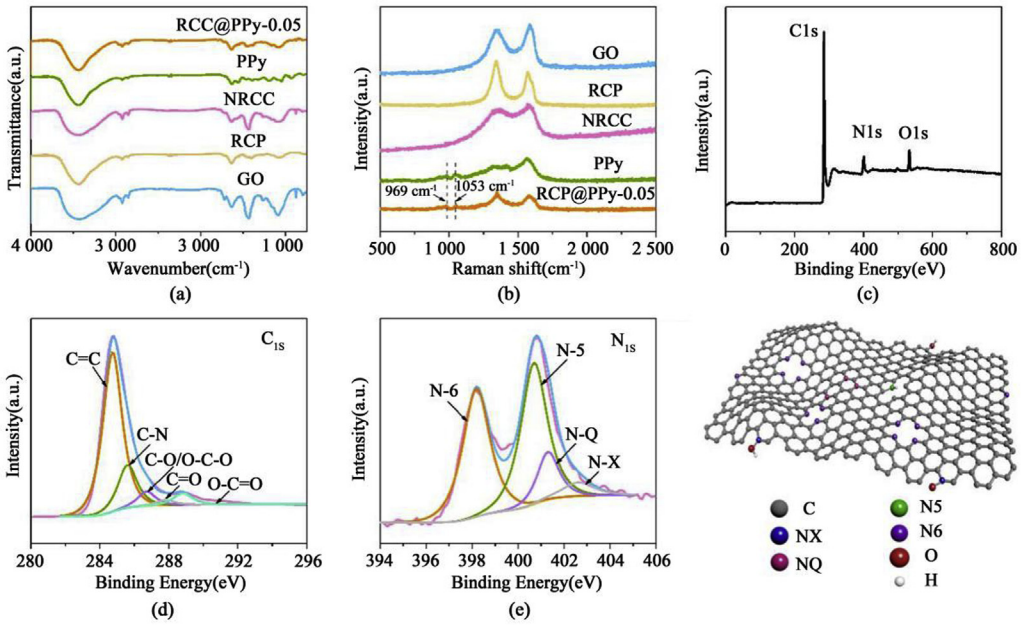

Fig. 3. (a) FTIR spectra and (b) Raman spectra of GO, RCP, PPy, RCP@PPy-0.05, and NRCC. (c) XPS survey spectrum for the NRCC. High-resolution XPS spectra of (d) N1s peak and (e) C1s peak. (f) Schematic of the nitrogen doping structure.

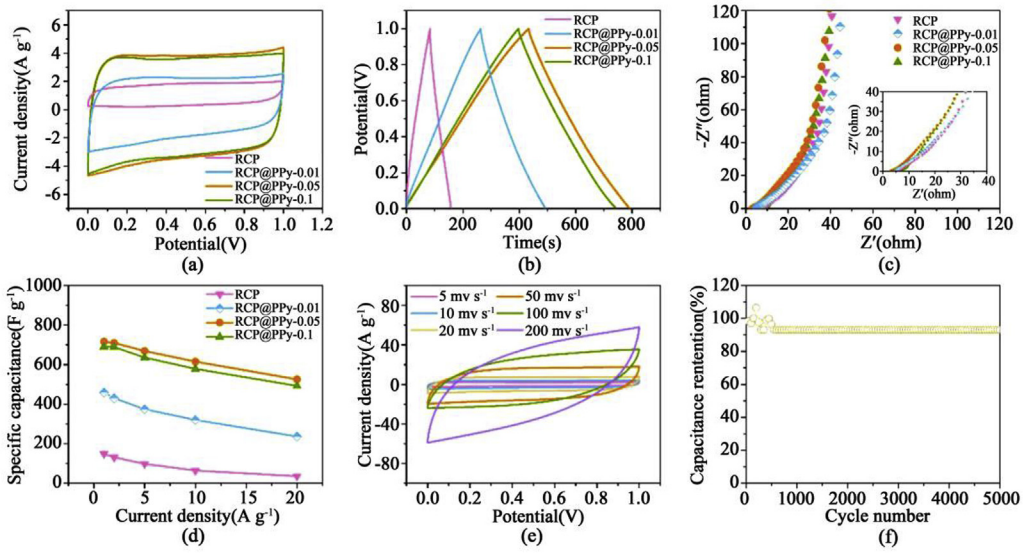

Fig. 4. Electrochemical performances of RCP and RCP@PPy-x (x = 0.01, 0.05, 0.1) based symmetric supercapacitor. (a) CV curves at 10 mV s^{-1}, (b) GCD curves at 1 A g^{-1}, (c) Nyquist plots, (d) Specific capacitance at various current densities, (e) CV curves of RCP@PPy-0.05, (f) Cyclic stability of RCP@PPy-0.05 at 5 A g^{-1}.

Pyrrole was subsequently polymerized on the GCP composite aerogel film, and RCP@PPy-x (where x represents the concentration of pyrrole, x = 0.01, 0.05, 0.1) composite aerogel film was obtained after polymerization and chemical reduction. N-doped RGO/CNT/CNF (NRCC) composite aerogel film can be produced by carbonization of RCP@PPy-0.05. During the carbonization process, PAN is turned into carbon nanofiber (CNF) and polypyrrole is pyrolyzed to realize N-doping.

The cross-sectional morphology of RCP and RCP@PPy-x aerogel film is shown in Fig. 2 and Fig. S2. As shown in Fig. 2a, the RCP has a porous structure consisting of two connected parts, an upper RGO/CNT aerogel and a bottom PAN nanofiber membrane. The upper RGO/CNT aerogel displays an interconnected macroporous structure (Fig. 2b), which benefits from the gel behavior of GO in the presence of CNT. Such a 3D skeleton structure facilitates the rapid transport of electrolyte ions and electrons, thereby accelerating the electrochemical reaction rate. It can be seen from Fig. 2c that the upper composite aerogel is closely connected to the bottom PAN nanofiber, indicating the film is integrated. The bottom PAN nanofiber layer shows a typical nanofiberous structure, with a fiber diameter of ~300 nm (Fig. 2d). Fig. 2e–h shows that the RCP@PPy-0.05 still maintains the overall structure of RCP after polymerization of pyrrole. Compared with RCP, the surface of the upper RGO/CNT aerogel, as well as the bottom PAN nanofiber, becomes rougher, indicating that PPy is uniformly coated on the RCP aerogel film. The SEM images of RCP@PPy-0.01 and RCP@PPy-0.1 reveal that PPy existed extensively in the 3D network, with the concentration of pyrrole monomer increased (Fig. S2). And the thermogravimetric analysis shows that the weight ratio of PPy in RCP@PPy-0.01, RCP@PPy-0.05 and RCP@ PPy −0.1 is 73.4, 77.5 and 89.4 wt%, respectively (Fig. S3, Table S1). In addition, the NRCC still exhibits a 3D interconnected macroporous structure, reflecting the excellent mechanical properties of the graphene 3D network skeleton. The carbon fibers aligned laterally at the bottom provide strong support for the upper nitrogen doped graphene aerogel (Fig. S4).

Fig. 3a shows the FTIR spectra of GO, RCP, PPy, RCP@PPy-0.05, and NRCC. The characteristic peaks of GO at 1087, 1267, 1720, and 1433 cm^{-1} belong to O–C–O, C–OH, C═O stretching vibration and –OH deformation vibration. As for RCP, the characteristic peaks of oxygen-containing functional groups become weak and disappear, indicating effective reduction of GO. NRCC also has C═C stretching vibration at 1637 cm^{-1}, but two unique peaks representing the C–N and the = C–N stretching vibration of the pyrrole ring appear at 1077 and 1433 cm^{-1}, confirming that the N atom was successfully incorporated into the graphene lattice. In the spectrum of PPy, the peaks ascribed to the C–H deformation vibration, C–N stretching vibration and C═C in-plane stretching vibration on the pyrrole rings are located at 1409, 1201, and 1563 cm^{-1}, respectively. And the characteristic doping state peak of PPy appears at 930 cm^{-1}. RCP@PPy-0.05 shows similar peaks to that of PPy, which proves that the RCP@PPy composite has been successfully prepared. The Raman spectra (Fig. 3b) of GO and RCP both have two peaks in the range of 1300 cm^{-1}-1400 cm^{-1} and 1500 cm^{-1}-1600 cm^{-1}, which are attributed to the D band and the G band, respectively, of the graphene [33–35]. The I_D/I_G values of GO and RCP are 0.96 and 1.11, respectively. The increase in the ratio indicates that the RCP has a greater degree of defects, which is related to the reduction of GO and the 3D structure of the sample itself [36]. The D band and the G band of the NGCC are not prominent, which may be associated with defects and disorder caused by N-doping. The RCP/PPy-0.05 showed the same characteristic peak as PPy at 969 cm^{-1} and 1053 cm^{-1}, indicating that PPy was successfully loaded on the aerogel. Fig. S5 shows the XRD patterns of GO, RCP@PPy-0.05, PPy, and NRCC. The diffraction peak of GO appears at 10.7°, corresponding to the (001) crystal plane, indicating the interlamellar spacing is 0.83 nm. RCP@PPy-0.05 exhibits a broad peak at around 25.2°, due to the combination of pure PPy (diffraction peak at about 21.4°) and amorphous carbon [34]. The NGCC has a broad peak at about 27°, suggesting that N-doping can result in poor crystallinity and an amorphous structure.

The chemical contents and nitrogen bonding configuration of the NRCC film was determined by XPS. As shown in Fig. 3c, the XPS spectrum of the NRCC demonstrates the presence of C, N, and O elements located at 284.9 eV, 399.9 eV and 532.6 eV, respectively. The N atom content in the NGCC is as high as 9.1 at% (Table S2). The C 1s spectrum can be deconvoluted into five individual peaks that are attributed to C–C, C–N, C–O, C═O, O–C═O at 284.7 eV, 285.6 eV, 286.7 eV, 287.8 eV and 288.8 eV, respectively (Fig. 3d) [37–39]. In addition, the high-resolution N 1s peaks reveal the existence of pyridinic N (N-6), pyrrolic N (N-5), quaternary N (N-Q) and oxidized N (N-X) at 398.2 eV, 400.7 eV, 401.3 eV and 402.6 eV, respectively (Fig. 3e). N-6 and N-5 are electrochemically active N atoms, which have the ability to contribute electron pairs. In addition, graphite N, as an electron acceptor, has electron affinity and can enhance the conductivity. These polarized N atoms, incorporated into the carbon lattice, can enhance the wettability of the electrolyte-electrode interface, accelerate the ion transport and undergo redox reactions, thus providing additional pseudocapacitance. Fig. 3f is a schematic diagram of the four N atom configurations in the carbon lattice.

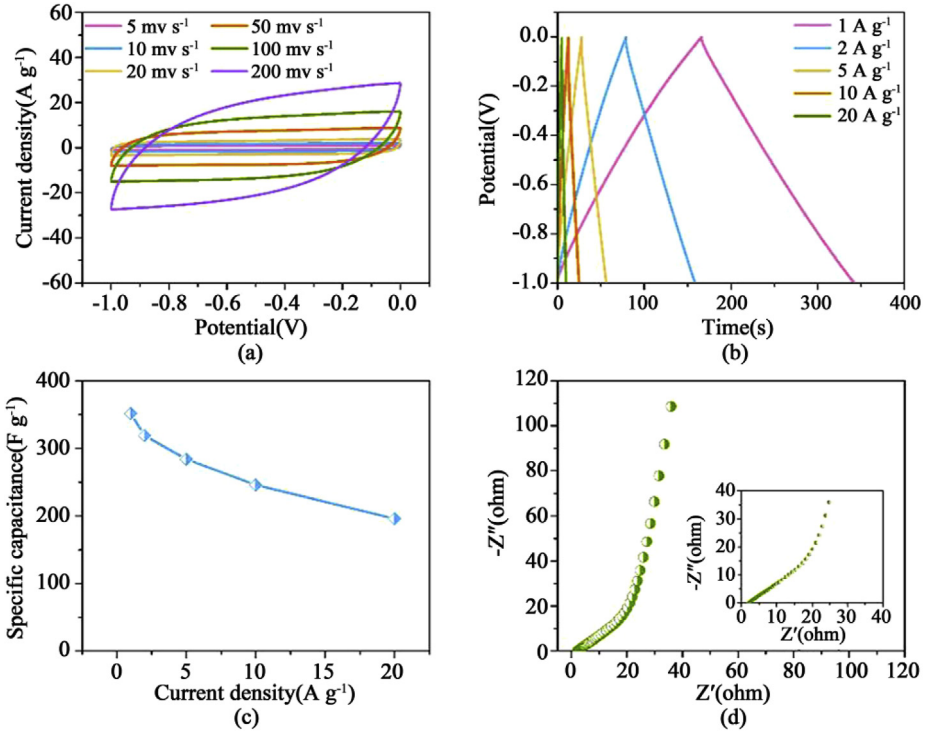

Fig. 5. Electrochemical performance of the NRCC based symmetric supercapacitor. (a) CV curves at different scan rates, (b) GCD curves at 1 A g^{-1}, (c) Specific capacitance at different current densities, (d) Nyquist plots.

3.2. Electrochemical performance of RCP@PPy-x based symmetric supercapacitor

RCP and RCP@PPy-x were assembled into symmetric supercapacitors and their electrochemical performance was explored in 0.5 M H_2SO_4 electrolyte (Fig. 4). Fig. 4a shows the CV curves of the RCP and RCP@PPy-x at a sweep rate of 10 mV s^{-1}. The CV profiles of all samples are nearly rectangular, indicating good electrochemical behavior. The area of the rectangle enclosed by the CV curve represents the specific capacitance [40]. It can be concluded that the RCP@PPy-0.05 has the largest specific capacitance value. When the current density is 1 A g^{-1}, the GCD curve is an almost symmetrical triangle and the voltage drop is not obvious at the beginning of the discharge, showing that the electrolyte ions are in good contact with the electrode material and have a high migration rate (Fig. 4b) [41]. According to equation (1), the specific capacitance values of GCP and GCP@PPy-x can be calculated as 148.6, 459.1, 716.1 and 690.1 F g^{-1}, respectively. Nyquist plots are recorded in Fig. 4c. It can be seen that there is no obvious semicircle in the high frequency region, suggesting that the charge-transfer resistance is small, while there is a nearly vertical line in the low frequency region, showing that the electrolyte ions can shuttle quickly in the electrode material, which is beneficial for accelerating the reaction rate [42–45]. This result is derived from the 3D porous framework structure, with the good electrical conductivity of GCP@PPy.

The rate capability is shown in Fig. 4d. The specific capacitance of all samples slowly decreases with the increasing current density. Even at the current density of 20 A g^{-1}, the RCP@PPy-0.05 still has a capacitance retention of 73.3% (525.1 F g^{-1}), demonstrating the desirable rate performance of the electrode material. This is due to the fact that the RGO/CNT aerogel has interconnected porous structures that provide a large enough contact area for PPy. The profile of the CV curve of the GCP@PPy-0.05 can still present a nearly rectangular profile at a sweep speed of 200 mV s^{-1}, indicating that the 3D network structure can provide sufficient channels for ion transport (Fig. 4e) [40]. Fig. 4f shows the cycling stability for the GCP@PPy-0.05. Finishing 5000 cycles of continuous charging and discharging, it still has a capacitance retention rate of 93.1%, exhibiting good cycling performance, which is due to the robust structure of the PAN nanofibers and the porous structure buffering the volume expansion of the PPy. The flexible substrate at the bottom gives strong support to the upper aerogel, thus, this double layer structure has excellent mechanical properties and can form a strong and effective transport channel for the electrolyte ions.

3.3. Electrochemical performance of the NGCC-based symmetric supercapacitor

The electrochemical performance of the NGCC-based symmetric supercapacitor is presented in Fig. 5. The CV curves of the NGCC shows a rectangular profile, which can still be retained at 200 mV s^{-1}, reflecting the rapid transfer rate of the electrolyte ions and electrons in the electrode material (Fig. 5a). The GCD curves of the NGCC are a nearly symmetrical triangle, indicating good rate performance (Fig. 5b) [46]. The NGCC can achieve a specific capacity of 351.6 F g^{-1} 1 A g^{-1}, and can maintain a capacitance retention rate of 55.7% at 20 A g^{-1} (Fig. 5c). This shows that the combination of nanofiber and aerogel is beneficial to accelerate the transport of ions and electrons, and N-doping can enhance the wettability of the electrode material, further accelerating the reaction rate [47]. The EIS measurements reflect that the equivalent series resistance (Rs) together with the charge-transfer resistance (Rct) of NGCC are small, suggesting a rapid and reversible Faraday reaction (Fig. 5d). Fig. S6 shows the capacitance retention of the NGCC during 5000 cycles. At the beginning of the cycle, as the number of charges and discharges increase, the electrolyte gradually penetrates the electrode material and more active sites of the N atom are added to the reaction, thus increasing the capacitance slightly as a result of the activation of the electrode material [48]. After that, the capacitance is kept at a stable level and can maintain a capacitance of 80.6% after 5000 cycles.

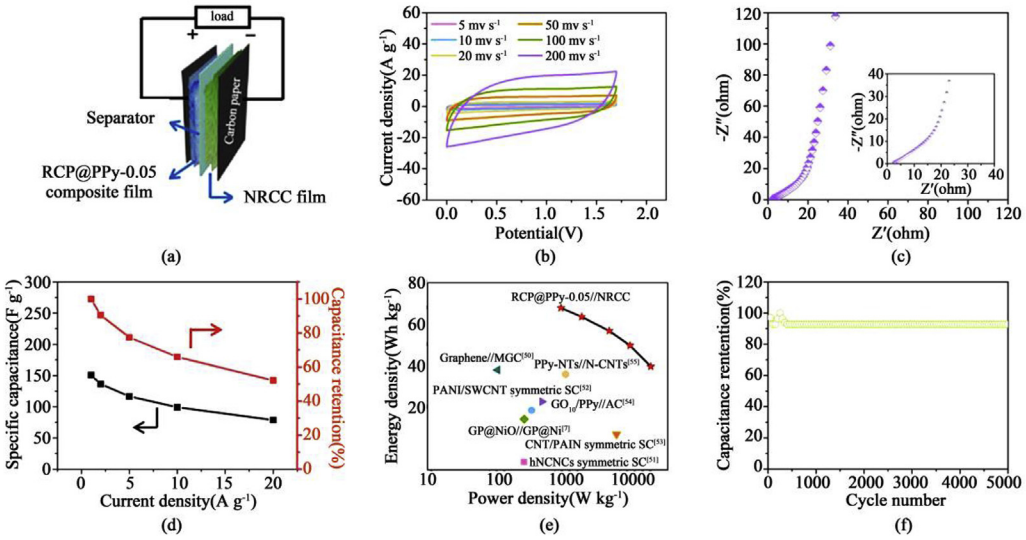

Fig. 6. Electrochemical test of the RCP@PPy-0.05//NRCC asymmetric device. (a) Schematic of the RCP@PPy-0.05//NRCC asymmetric device, (b) CV curves of the asymmetric cell at various scan rates, (c) Nyquist plots, (d) Specific capacitance and the related capacitance retention, (e) Ragone plots, (f) Cyclic stability at 5 A g^{-1}.

3.4. Asymmetric supercapacitor performance

Studies have shown that expanding the voltage window can improve the energy density. To achieve a larger voltage window, we fabricated an RCP@PPy-0.05//NRCC based asymmetric supercapacitor using RCP@PPy-0.05 and NRCC as the positive electrode and the negative electrode, respectively (illustrated in Fig. 6a). The asymmetric device can realize a voltage window of 1.7 V. Fig. 6b shows the CV curves of the device under different sweep speeds. The nearly rectangular shape can still be maintained at 200 mV s^{-1}, indicating the fast electrolyte ion transport rate. Impedance data shows as a nearly vertical line and as an inconspicuous semicircle in the low and high frequency regions, respectively (Fig. 6c), demonstrating that the electrolyte ions can quickly shuttle between the electrode materials to accelerate the reaction rate [49–51]. The device can achieve a specific capacity of 150.9 F g^{-1} at 1 A g^{-1}. It can be seen from Fig. 6d that even if the current density increases to 20 A g^{-1}, the device can still retain 52.2% of its capacitance, demonstrating its desirable rate performance. According to the GCD curve in Fig. S7 and equations (3) and (4), we have calculated the power density and the energy density of the device and presented them in a Ragone plot (Fig. 6e). A maximum energy density of 60.6 W h kg^{-1} can be achieved at a power density of 850.2 W kg^{-1}, and a maximum power density is 16.9 kW kg^{-1} at 31.6 W h kg^{-1}. The energy density performance has advantage over those previously reported symmetric and asymmetric supercapacitors, as listed in Table S3, such as PANI/SWCNT (the energy density at 320.5 W kg^{-1} is 19.4 W h kg^{-1}) [52], CNT/PANI (the energy density at 5.4 kW kg^{-1} is 14.9 W h kg^{-1}) [53], GO_{10}/PPy//AC (the energy density at 453.9 W kg^{-1} is 21.4 W h kg^{-1}) [54], and PPy-NTs//N-CNTs (the energy density at 998.6 W kg^{-1} is 28.9 W h kg^{-1}) [55]. The cycling performance is shown in Fig. 6f, with a capacitance retention of 92.8% after 5000 cycles. The synergistic effects of the porous skeleton structure and the introduction of pseudocapacitance provide new possibilities for devices with high operating voltage and excellent performance.

4. Conclusion

In summary, we demonstrate a scalable synthetic route to fabricate a novel 3D graphene-based aerogel film and present its applications in binder-free supercapacitors. GO/CNT hydrogel was coated on an electrospun polyacrylonitrile (PAN) nanofiber membrane to construct a 3D porous structure, then free-standing GO/CNT/PAN (GCP) aerogel film with a two-layered structure was obtained by freeze-drying. In the GCP aerogel film, the bottom PAN nanofiber membrane provides flexibility and strong support for the upper aerogel, and the upper GO/CNT aerogel displays an interconnected macroporous structure that provides a rapid transmission channel for the electrolyte ions and electrons. Polypyrrole (PPy) was loaded on the GCP aerogel film to introduce pseudocapacitance, and nitrogen-doped RGO/CNT/carbon nanofiber (NRCC) composite aerogel film was obtained after further pyrolysis. The resultant RCP@PPy-0.05 symmetrical supercapacitor has the highest capacitance of 716.1 F g^{-1} at 1 A g^{-1}, and it still has a capacitance retention of 73.3% (525.1 F g^{-1}) at 20 A g^{-1}, demonstrating the desirable rate performance of the electrode material. The NGCC based symmetric device displays a specific capacity of 351.6 F g^{-1} at 1 A g^{-1} and the capacitance retention is 55.7% at 20 A g^{-1}. Furthermore, RCP@PPy-0.05//NRCC based asymmetric supercapacitors operate stably under a 1.7 V voltage window. The device can achieve a specific capacity of 150.9 F g^{-1} at 1 A g^{-1}, with a capacitance retention of 92.8% after 5000 cycles. The maximum energy density can reach 60.6 W h kg^{-1} at a power density of 850.2 W kg^{-1}. This strategy provides a scalable way to prepare flexible electrode materials for supercapacitors with high energy density.

Declaration of competing interest

None.

Acknowledgements

The authors are grateful for the financial support from the National Natural Science Foundation of China (21704014, 21674019), Fundamental Research Funds for Central Universities (2232019A3-03), the Program of Shanghai Academic Research Leader (17XD1400100), the Shanghai Sailing Program (17YF1400200), the Shanghai Municipal Education Commission (17CG33).

Appendix A. Supplementary data

Supplementary data to this article can be found online at https://doi.org/10.1016/j.nanoms.2020.03.003.

References

[1] X. Yang, J. Zhu, L. Qiu, et al., Bioinspired effective prevention of restacking in multilayered graphene films: towards the next generation of high-performance supercapacitors, Adv. Mater. 23 (2011) 2833–2838.
[2] M. Tian, J. Wu, R. Li, et al., Fabricating a high-energy-density supercapacitor with asymmetric aqueous redox additive electrolytes and free-standing activated-carbon-felt electrodes, Chem. Eng. J. 363 (2019) 183–191.
[3] K. Shu, C. Wang, S. Li, et al., Flexible free-standing graphene paper with interconnected porous structure for energy storage, J. Mater. Chem. 3 (2015) 4428–4434.
[4] Z. Zhang, M. Liu, X. Tian, et al., Scalable fabrication of ultrathin free-standing graphene nanomesh films for flexible ultrafast electrochemical capacitors with AC line-filtering performance, Nano Energy 50 (2018) 182–191.
[5] J. Tang, P. Yuan, C. Cai, et al., Combining nature-inspired, graphene-wrapped flexible electrodes with nanocomposite polymer electrolyte for asymmetric capacitive energy storage, Adv. Energy Mater. 6 (2016) 1600813–1600823.
[6] F. Güneş, H. Shin, C. Biswas, et al., Layer-by-layer doping of few-layer graphene film, ACS Nano 4 (2010) 4595–4600.
[7] X. Jiao, Q. Hao, X. Xia, et al., Free-Standing hybrid graphene paper encapsulating nanostructures for high cycle-life supercapacitors, Chemsuschem 11 (2018) 907–915.
[8] Varzi, R. Raccichini, M. Marinaro, et al., Probing the characteristics of casein as green binder for non-aqueous electrochemical double layer capacitors' electrodes, J. Power Sources 326 (2016) 672–679.
[9] X. Wang, Y. Zhang, C. Zhi, et al., Three-dimensional strutted graphene grown by substrate-free sugar blowing for high-power-density supercapacitors, Nat. Commun. 4 (2013).
[10] J. Chen, J. Xu, S. Zhou, et al., Nitrogen-doped hierarchically porous carbon foam: a free-standing electrode and mechanical support for high-performance supercapacitors, Nano Energy 25 (2016) 193–202.
[11] X. Cao, Z. Yin, H. Zhang, et al., Three-dimensional graphene materials: preparation, structures and application in supercapacitors, Energy Environ. Sci. 7 (2014) 1850–1865.
[12] X. Cao, Y. Shi, W. Shi, et al., Preparation of novel 3D graphene networks for supercapacitor applications, Small 7 (2011) 3163–3168.
[13] E. Fiset, T.E. Rufford, M. Seredych, et al., Comparison of melamine resin and melamine network as precursors for carbon electrodes, Carbon 81 (2015) 239–250.
[14] W. Ouyang, J. Sun, J. Memon, et al., Scalable preparation of three-dimensional porous structures of reduced graphene oxide/cellulose composites and their application in supercapacitors, Carbon 62 (2013) 501–509.
[15] G. Zhu, C. Xi, Y. Liu, et al., CN foam loaded with few-layer graphene nanosheets for high-performance supercapacitor electrodes, J. Mater. Chem. 3 (2015) 7591–7599.
[16] Z. Wang, X. Shen, M. Akbari Garakani, et al., Graphene Aerogel/Epoxy composites with exceptional anisotropic structure and properties, ACS Appl. Mater. Interfaces 7 (2015) 5538–5549.
[17] M.A. Worsley, T.T. Pham, A. Yan, et al., Synthesis and characterization of highly crystalline graphene aerogels, ACS Nano 8 (2014) 11013–11022.
[18] G. Wang, X. Sun, F. Lu, et al., Flexible pillared graphene-paper electrodes for high-performance electrochemical supercapacitors, Small 8 (2012) 452–459.
[19] Y. Zhu, S. Murali, M.D. Stoller, et al., Carbon-based supercapacitors produced by activation of graphene, Science 332 (2011) 1537–1541.
[20] X. Liu, J. Xi, B.B. Xu, et al., A high-performance direct methanol fuel cell technology enabled by mediating high-concentration methanol through a graphene aerogel, Small Methods 2 (2018) 1800138–1800143.
[21] J. Zhao, R. Pan, R. Sun, et al., High-conductivity reduced-graphene-oxide/copper aerogel for energy storage, Nano Energy 60 (2019) 760–767.
[22] H. Bai, C. Li, X. Wang, et al., On the gelation of graphene oxide, J. Phys. Chem. C 115 (2011) 5545–5551.
[23] X. Yang, C. Cheng, Y. Wang, et al., Liquid-mediated dense integration of graphene materials for compact capacitive energy storage, Science 341 (2013) 534–537.
[24] F. Tristán-López, A. Morelos-Gómez, S.M. Vega-Díaz, et al., Large area films of alternating graphene-carbon nanotube layers processed in water, ACS Nano 7 (2013) 10788–10798.
[25] W. Yao, R. Mao, W. Gao, et al., Piezoresistive effect of superelastic graphene aerogel spheres, Carbon 158 (2019) 418–425.
[26] H. Sun, Z. Xu, C. Gao, Multifunctional, ultra-flyweight, synergistically assembled carbon aerogels, Adv. Mater. 25 (2013) 2554–2560.
[27] J. Liang, Y. Huang, J. Oh, et al., Electromechanical actuators based on graphene and graphene/Fe_3O_4 hybrid paper, Adv. Funct. Mater. 21 (2011) 3778–3784.
[28] X. Huang, K. Qian, J. Yang, et al., Functional nanoporous graphene foams with controlled pore sizes, Adv. Mater. 24 (2012) 4419–4423.
[29] Q. Wu, Y. Xu, Z. Yao, et al., Supercapacitors based on flexible graphene/polyaniline nanofiber composite films, ACS Nano 4 (2010) 1963–1970.
[30] Y. Liu, J. Zhou, X. Zhang, et al., Synthesis, characterization and optical limiting property of covalently oligothiophene-functionalized graphene material, Carbon 47 (2009) 3113–3121.
[31] J. Yan, T. Wei, B. Shao, et al., Preparation of a graphene nanosheet/polyaniline composite with high specific capacitance, Carbon 48 (2010) 487–493.
[32] W.S. Hummers, R.E. Offeman, Preparation of graphitic oxide, J. Am. Chem. Soc. 80 (1958), 1339-1339.
[33] L. Liu, Z. Niu, L. Zhang, et al., Nanostructured graphene composite papers for highly flexible and foldable supercapacitors, Adv. Mater. 26 (2014) 4855–4862.
[34] D. Zhang, X. Zhang, Y. Chen, et al., Enhanced capacitance and rate capability of graphene/polypyrrole composite as electrode material for supercapacitors, J. Power Sources 196 (2011) 5990–5996.
[35] A.L.M. Reddy, A. Srivastava, S.R. Gowda, et al., Synthesis of nitrogen-doped graphene films for lithium battery application, ACS Nano 4 (2010) 6337–6342.
[36] D. Geng, Y. Chen, Y. Chen, et al., High oxygen-reduction activity and durability of nitrogen-doped graphene, Energy Environ. Sci. 4 (2011) 760–764.
[37] Z. Sheng, L. Shao, J. Chen, et al., Catalyst-free synthesis of nitrogen-doped graphene via thermal annealing graphite oxide with melamine and its excellent electrocatalysis, ACS Nano 5 (2011) 4350–4358.
[38] G. Wang, H. Wang, X. Lu, et al., Solid-state supercapacitor based on activated carbon cloths exhibits excellent rate capability, Adv. Mater. 26 (2014) 2676–2682.
[39] M. Yang, Y. Zhong, J. Bao, et al., Achieving battery-level energy density by constructing aqueous carbonaceous supercapacitors with hierarchical porous N-rich carbon materials, J. Mater. Chem. 3 (2015) 11387–11394.
[40] C. Liu, Z. Yu, D. Neff, et al., Graphene-based supercapacitor with an ultrahigh energy density, Nano Lett. 10 (2010) 4863–4868.
[41] W. Qian, F. Sun, Y. Xu, et al., Human hair-derived carbon flakes for electrochemical supercapacitors, Energy Environ. Sci. 7 (2014) 379–386.
[42] Y. Cheng, L. Huang, X. Xiao, et al., Flexible and cross-linked N-doped carbon nanofiber network for high performance freestanding supercapacitor electrode, Nano Energy 15 (2015) 66–74.
[43] X. Ma, L. Gan, M. Liu, et al., Mesoporous size controllable carbon microspheres and their electrochemical performances for supercapacitor electrodes, J. Mater. Chem. 2 (2014) 8407–8415.
[44] W. Luo, B. Wang, C.G. Heron, et al., Pyrolysis of cellulose under ammonia leads to nitrogen-doped nanoporous carbon generated through methane formation, Nano Lett. 14 (2014) 2225–2229.
[45] H. Wang, Q. Hao, X. Yang, et al., Effect of graphene oxide on the properties of its composite with polyaniline, ACS Appl. Mater. Interfaces 2 (2010) 821–828.
[46] L. Fan, G. Liu, J. Wu, et al., Asymmetric supercapacitor based on graphene oxide/polypyrrole composite and activated carbon electrodes, Electrochim. Acta 137 (2014) 26–33.
[47] L. Chen, X. Zhang, H. Liang, et al., Synthesis of nitrogen-doped porous carbon nanofibers as an efficient electrode material for supercapacitors, ACS Nano 6 (2012) 7092–7102.
[48] P.P. Li, Z.Y. Jin, L.L. Peng, et al., Stretchable all-gel-state fiber-shaped supercapacitors enabled by macromolecularly interconnected 3D graphene/nanostructured conductive polymer hydrogels, Adv. Mater. 30 (2018) 1800124–1800129.
[49] Y. Shao, M.F. El-Kady, C. Lin, et al., 3D freeze-casting of cellular graphene films for ultrahigh-power-density supercapacitors, Adv. Mater. 28 (2016) 6719–6726.
[50] Z. Wu, W. Ren, D. Wang, et al., High-energy MnO_2 Nanowire/Graphene and graphene asymmetric electrochemical capacitors, ACS Nano 4 (2010) 5835–5842.
[51] J. Zhao, H. Lai, Z. Lyu, et al., Hydrophilic hierarchical nitrogen-doped carbon nanocages for ultrahigh supercapacitive performance, Adv. Mater. 27 (2015) 3541–3545.
[52] F. Liu, S. Luo, D. Liu, et al., Facile processing of free-standing polyaniline/SWCNT film as an integrated electrode for flexible supercapacitor application, ACS Appl. Mater. Interfaces 9 (2017) 33791–33801.
[53] W. Zhao, Y. Li, S. Wu, et al., Highly stable carbon nanotube/polyaniline porous network for multifunctional applications, ACS Appl. Mater. Interfaces 8 (2016) 34027–34033.
[54] L. Fan, G. Liu, J. Wu, et al., Asymmetric supercapacitor based on graphene oxide/polypyrrole composite and activated carbon electrodes, Electrochim. Acta 137 (2014) 26–33.
[55] D.P. Dubal, N.R. Chodankar, Z. Caban-Huertas, et al., Synthetic approach from polypyrrole nanotubes to nitrogen doped pyrolyzed carbon nanotubes for asymmetric supercapacitors, J. Power Sources 308 (2016) 158–165.